

Quantification of water exchange across the blood-brain barrier using noncontrast MR fingerprinting

Emma L. Thomson^{1,2}  | Elizabeth Powell¹ 

Claudia A. M. Gandini Wheeler-Kingshott^{2,3,4}  | Geoff J. M. Parker^{1,2,5} 

¹Centre for Medical Image Computing, Department of Medical Physics and Biomedical Engineering, University College London, London, UK

²NMR Research Unit, Queen Square MS Centre, Department of Neuroinflammation, UCL Queen Square Institute of Neurology, Faculty of Brain Sciences, London, UK

³Department of Brain & Behavioural Sciences, University of Pavia, Pavia, Italy

⁴IRCCS Mondino Foundation, Pavia, Italy

⁵Bioxydyn Limited, Manchester, UK

Correspondence

Geoff J. M. Parker, Centre for Medical Image Computing, University College London, 90 High Holborn, London WC1V 6LJ, UK.

Email: geoff.parker@ucl.ac.uk

Funding information

The National Institute for Health and Care Research University College London Hospitals Biomedical Research Centre, Grant/Award Number: BRC704/CAP/CGW; EU Horizon2020 Research and Innovation Action Grants Human Brain Project, Grant/Award Number: 945539(SGA3); Rosetrees Trust, Grant/Award Numbers: PGL22/100041, PGL21/10079; EPSRC, Grant/Award Number: EP/S031510/1; EPSRC Centre for Doctoral Training in Intelligent, Integrated Imaging In Healthcare (i4health), Grant/Award Number: EP/S021930/1; MRC, Grant/Award Number: MR/S026088/1

Abstract

Purpose: A method is proposed to quantify cerebral blood volume (v_b) and intravascular water residence time (τ_b) using MR fingerprinting (MRF), applied using a spoiled gradient echo sequence without the need for contrast agent.

Methods: An in silico study optimized an acquisition protocol to maximize the sensitivity of the measurement to v_b and τ_b changes. Its accuracy in the presence of variations in $T_{1,t}$, $T_{1,b}$, and B_1 was evaluated. The optimized protocol (scan time of 19 min) was then tested in an exploratory healthy volunteer study (10 volunteers, mean age 24 ± 3 , six males) at 3 T with a repeat scan taken after repositioning to allow estimation of repeatability.

Results: Simulations show that assuming literature values for $T_{1,b}$ and $T_{1,t}$, no variation in B_1 , while fitting only v_b and τ_b , leads to large errors in quantification of v_b and τ_b , regardless of noise levels. However, simulations also show that matching $T_{1,t}$, $T_{1,b}$, B_1^+ , v_b and τ_b , simultaneously is feasible at clinically achievable noise levels. Across the healthy volunteers, all parameter quantifications fell within the expected literature range. In addition, the maps show good agreement between hemispheres suggesting physiologically relevant information is being extracted. Expected differences between white and gray matter $T_{1,t}$ ($p < 0.0001$) and v_b ($p < 0.0001$) are observed, $T_{1,b}$ and τ_b show no significant differences, $p = 0.4$ and $p = 0.6$, respectively. Moderate to excellent repeatability was seen between repeat scans: mean intra-class correlation coefficient of $T_{1,t}$: 0.91, $T_{1,b}$: 0.58, v_b : 0.90, and τ_b : 0.96.

Conclusion: We demonstrate that regional simultaneous quantification of v_b , τ_b , $T_{1,b}$, $T_{1,t}$, and B_1^+ using MRF is feasible in vivo.

KEYWORDS

blood brain barrier, MR fingerprinting, water exchange

1 | INTRODUCTION

Integrity of the blood brain barrier (BBB), the semi-permeable barrier that separates the blood in vessels from the extracellular tissue in the central nervous system,¹ is vital for supplying the brain with nutrients and solutes while protecting the neural tissue from toxins and pathogens. Breakdown of the BBB allows these toxic substances into the brain and is thought to be a key component in the progression of multiple neurological diseases.²

The ability to quantify physical parameters associated with BBB integrity would give insight into early disease and may be valuable for monitoring progression and response to treatment. A number of solutions for the detection of breakdown of the BBB using MRI have been proposed; currently the most widely available method, dynamic control enhanced-MRI,^{3,4} requires a gadolinium-based contrast agent, and is best suited to quantifying severe damage, as it measures the transfer of the relatively large contrast agent complex over the BBB. Aside from the fact that gadolinium-based contrast agent carries some health-related contraindications,⁵ it suffers from poor sensitivity and a low signal-to-noise ratio (SNR) when trying to assess subtle damage.^{6,7}

An alternative approach, which may offer greater sensitivity than dynamic control enhanced-MRI, while also avoiding the use of gadolinium-based contrast agents, is to measure exchange of the smaller, and endogenously abundant, water molecules across the BBB. However, existing water exchange techniques, such as those based on arterial spin labeling^{8–10} or diffusion MRI methods such as filter exchange imaging,^{11,12} also suffer from low SNR.

A technique that has been shown to boost SNR and sensitivity in a range of quantitative MRI settings is MR fingerprinting (MRF). MRF exploits the signal response of tissues when repeatedly exposed to radiofrequency (RF) pulses of different amplitudes at varying intervals.^{13–15} Multiple sequence repetitions are performed consecutively, generating a signal that is characteristic of a unique set of tissue properties. These voxel-wise responses are compared with entries in a dictionary of simulated responses calculated from a set of known parameters, allowing maps of multiple parameters to be extracted simultaneously and efficiently.

Here, we propose, for the first time, using MRF to quantify BBB water exchange. We propose a technique that uses an RF spoiled gradient echo-MRF sequence to enable the simultaneous quantification of cerebral blood volume (v_b), intravascular residence time (τ_b , the inverse of water exchange rate), intravascular T_1 ($T_{1,b}$), extravascular T_1 ($T_{1,t}$), and B_1 multiplication factor, B_1^+ , without the use of contrast agent.

Through an in silico study an acquisition protocol was optimized. The accuracy and sensitivity of the measurement in the presence of variations in intravascular T_1 , extravascular T_1 , and B_1^+ was evaluated. The optimized protocol was then tested in a healthy volunteer study to determine feasibility and repeatability.

2 | METHODS

2.1 | Simulations and optimization

A three-dimensional array of spin isochromats was simulated assuming a two-site exchange system between intra and extravascular pools, with defined compartmental volumes and a semipermeable barrier, representing the BBB, allowing for two-way exchange. A singular, spatially nonuniform, voxel was modeled, described by a grid of isochromats, visualized in Figure 1. The Bloch equations were used to simulate signals arising from this array and its magnetization evolution over time. The isochromats within the intravascular compartment had a residence time, τ_b , dictating how long on average they spent in the vasculature. Exchange was simulated by outlining a probability of exchange at a given time step for each isochromat in the vasculature given by:

$$P(t) = 1 - e^{-(t/\tau_b)}, \quad (1)$$

where the probability of exchange of an isochromat at time t is one minus the exponential of the negative ratio of the

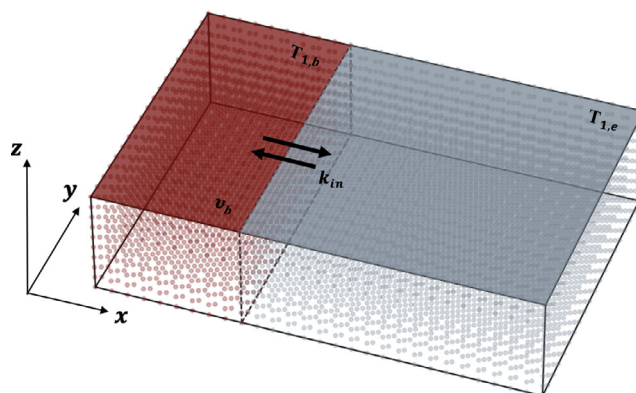


FIGURE 1 Grid array of isochromats subject to Bloch equation magnetization changes, in which a percentage (v_b) are governed by $T_{1,b}$ (the blood compartment in red) and the remainder are governed by $T_{1,t}$ (the tissue compartment in gray). Limited exchange occurs between the two compartments with the probability of exchange governed by the mean intravascular residence time ($\tau_b = 1/k_{in}$). Exchange influx and efflux is assumed to be equal. Along the z dimension a variation in flip angle magnitude was applied to reflect the slice profile.

total time the spin has been present in the vasculature over the mean residence time. Diffusion was assumed to occur freely within each compartment so the exchanging isochromat from the intravascular compartment would exchange with a random isochromat from within the extravascular compartment. Volume fractions were considered constant, so all exchange is two way: exchanging isochromats “swap” compartments while retaining magnetization history. After exchange, the cumulative probability of exchange for each exchanging isochromat is reset to zero. Simulated signals were generated first in quadrature and then summed such that the resultant transverse magnitude data was stored as the measured signal. The code used in this study is available at https://github.com/EmmaThomson/MRFSGRE_BBB. Not including flow in the dictionary was found to non-significantly impact the quality of quantification. This can be seen in Figure S1.

Along the z-direction the applied flip angle varies according to the imaging sequence slice profile. Slice profile was calculated using a separate Bloch equation simulation¹⁶ using the known characteristics of the applied RF pulse. To reduce the number of isochromats simulated, the slice profile was assumed to be symmetrical so only half of the profile was sampled and the resultant signal magnitude multiplied by two.

Optimization was performed using a branch and bound algorithm¹⁷ such that the variations of α and TR were optimized to maximize the difference between signals at the extremes of the range of healthy τ_b values ($200 \text{ ms} \leq \tau_b \leq 1600 \text{ ms}$)⁸ across a full MRF signal evolution. For each combination of MRF parameters tested, a signal evolution for a MRF sequence with 500 TRs was generated at either end of the τ_b range. The optimal set of sequence parameters were the ones that maximized the inner product between the two signal evolutions over time. $T_{1,t}$ was fixed at 1300 ms,^{18,19} and $T_{1,b}$ at 1700 ms,²⁰ mimicking a gray matter voxel at 3 T. Variation of α and TR was limited to predetermined shapes, with amplitude and width allowed to be optimized to allow for a computationally feasible search space.

The flip angle was varied to give a periodic positive sinusoidal variation in which the even peaks were lower than the odd, emulating the flip angle design in the original MRF paper,¹³ using the equation:

$$\alpha_N = \left| \alpha_{\max} \times \left(3 \times \sin\left(\frac{N}{w_\alpha}\right) + \sin\left(\frac{N}{w_\alpha}\right)^2 \right) \right|, \quad (2)$$

where N is the N th repetition of the applied sequence, and α_{\max} and w_α are the parameters that govern the maximum height of the peaks (degrees) and the width of the periodic variation (# of TRs), respectively. Optimization bounds

on these parameters were ($20 \leq \alpha_{\max} \leq 88$) [degrees] and ($5\pi \leq w_\alpha \leq 200\pi$) [# of α].

The variation in TR was sinusoidal governed by:

$$\text{TR}_N = \frac{1}{2} \left((\text{TR}_{\max} - \text{TR}_{\min}) \sin\left(\frac{Nf}{2\pi}\right) + (\text{TR}_{\min} + \text{TR}_{\max}) \right), \quad (3)$$

where f is the frequency that governs the period of the sinusoidal variation [$(\# \text{ of } \alpha)^{-1}$], and TR_{\min} (ms) and TR_{\max} (ms) govern its range. Optimization limits for these parameters are: ($1 \leq T \leq 200$) [$(\# \text{ of } \alpha)^{-1}$], ($4 \leq \text{TR}_{\min} \leq 200$) (ms) and ($9 \leq \text{TR}_{\max} \leq 200$) (ms). An upper boundary was imposed on the possible repetition time such that a 2000 TR sequence with a fully sampled center of k-space could be acquired in a clinically feasible timeframe (For a scan time of less than 20 min, $\text{TR}_{\max} = 200$ ms). TR lower bound was dictated by scanner sequence implementation lower limits ($\text{TR}_{\min} = 4$ ms). These variation parameters can be visualized in Figure 2A,B.

Optimization was performed three times with 2000 TRs: the best of these three repeats was chosen to be the optimum set of parameters.

To test these simulations three sets of experiments were performed. For each experiment a dictionary was generated with a range of noise levels to test the matching sensitivity to noise: this was repeated 50 times for each dictionary to allow for statistical analysis of the quality of the match to be performed. Quantification was said to have failed when the mean difference in matched value from the ground truth was larger than half a dictionary step size.

A two-dimensional (2D) dictionary was generated with variation in blood volume from 1% to 10% in steps of 1%, denoted $v_b = [\text{min} = 1 : \text{step} = 1 : \text{max} = 10]\%$ and mean residence time of water in the intravascular compartment, $\tau_b = [200 : 100 : 1600]$ ms. Three experiments were then performed: first, this 2D dictionary was matched against a 2D data set with the same variation to test the sensitivity of these variations to noise. Next, a sample data set with variation along five dimensions (5D), v_b ($[1 : 1 : 10]\%$), τ_b ($[200 : 100 : 1600]$ ms), intravascular T_1 : $T_{1,b}$ ($[1500 : 200 : 1900]$ ms), extravascular T_1 : $T_{1,t}$ ($[1000 : 200 : 2000]$ ms), and relative B_1^+ : ($[0.8 : 0.1 : 1.2]$), was matched to the 2D dictionary containing variation in v_b and τ_b only, with fixed values of $T_{1,b}$, $T_{1,t}$, and B_1^+ from the literature, to explore the robustness of matching when these parameters are not known a priori. Finally, the 5D sample was matched to a 5D dictionary with the same variation as the sample data set to test the feasibility of determining each parameter simultaneously. Variations in each parameter were chosen to encapsulate healthy ranges for both white and gray matter.^{8,18–28}

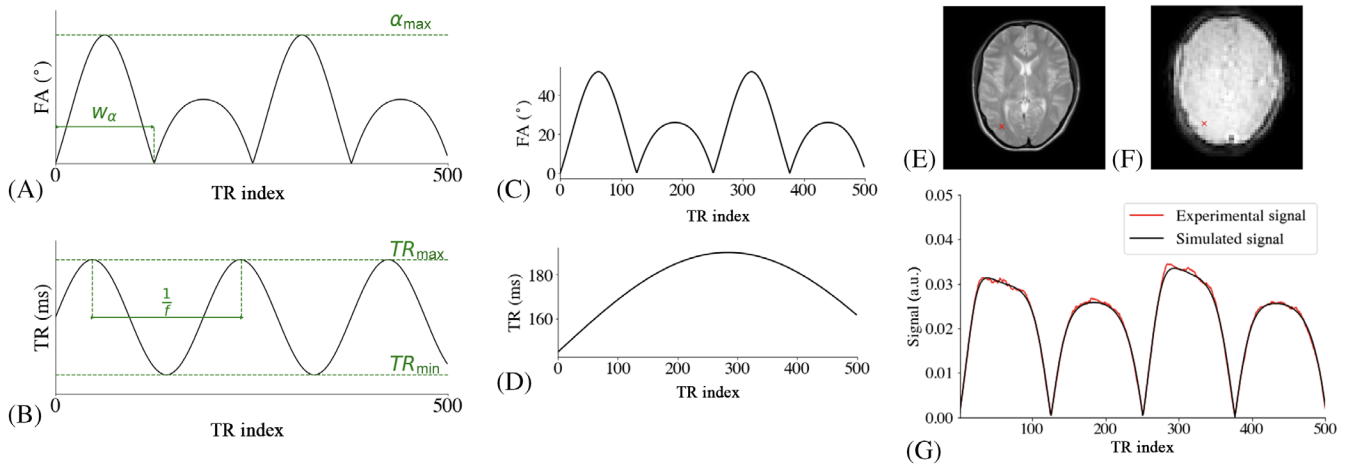


FIGURE 2 (A) Representative plots of the variations of the flip angle and (B) repetition time over five hundred consecutive repetitions of the sequence. The optimizable parameters that modify these variations are indicated in green. (C) Partial visualization of optimal variation in flip angle (labelled FA, identical to α) and (D) repetition time (TR) used for the first 500 acquisition steps: this variation repeats for the remaining TRs. The signals generated by these variations are matched to a precomputed dictionary. An example voxel marked in red on (E) a T_2 -weighted anatomy scan and (F) a raw MR fingerprinting image (image 100/2000) was isolated. (G) Shows this single voxel signal plotted against its closest dictionary match. [$T_{1,t}$:1300 ms, $T_{1,b}$:1700 ms, B_1^+ :0.78, v_b :2 %, τ_b :1200 ms].

2.1.1 | Noise metric

We modeled noise as a zero-mean complex Gaussian with SD σ_G on each isochromat. Each isochromat has an equilibrium magnetization of unity such that $\sigma_G = 0.01$ is equivalent to 1% noise. MRF signals however, seldom recover close to the equilibrium value: across a coarse, broad scope dictionary, the average signal value was 13.04% of the equilibrium value. For this MRF implementation we therefore define the SNR as:

$$\text{SNR} = \frac{13.04}{100\sigma_G}. \quad (4)$$

2.2 | Healthy volunteer testing

2.2.1 | Acquisition

Ten healthy volunteers (19–29 years old, mean age: 24 ± 3 years, six male) were recruited in accordance with the local Institutional Review Board guidelines with informed written consent. Each individual was scanned at 3 T on a Philips Ingenia system using a T1-fast field echo (T1-FFE, RF-spoiled gradient echo) acquisition with an MRF sequence of 2000 TRs, FOV = 224 mm \times 244 mm, reconstructed matrix = 64 \times 64, slice thickness = 5 mm, $TE = 2$ ms, fully sampled variable density spiral readout, SPIR fat saturation, with variation in α and TR as outlined in Figure 2 C,D, scan time = 19:27. A single central axial slice was acquired. A higher resolution single slice T_2 -weighted (Turbo Spin Echo, FOV = 224 mm \times 244 mm,

reconstructed matrix = 560 \times 560, voxel size = 3.5 mm \times 3.5 mm, slice thickness = 5 mm, $TE = 80$ ms, scan time = 1:48) and three-dimensional T_1 -weighed image (T1-FFE, FOV = 240 mm \times 240 mm, reconstructed matrix = 256 \times 256, slice thickness = 5 mm, $TE = 1.854$ ms, number of slices = 55, scan time = 3:22) were also acquired at the same location for segmentation and analysis. A repeat scan was performed within the same session as the initial scans after repositioning of the subject to allow assessment of parameter scan-rescan repeatability.

2.2.2 | Preprocessing

Brain extraction was done using FSL BET,²⁹ an initial affine linear registration performed using FLIRT,^{30,31} a subsequent non-linear registration using FNIRT,^{32,33} and segmentation performed using SynthSeg.³⁴ As large voxel sizes lead to partial volume effects, partial volume segmentations for white and gray matter were thresholded so that only voxels that contained 90% of the respective tissue were used in the calculation of regional means.

2.2.3 | Dictionary and matching

A 5D dictionary with around 0.65 million entries was generated for matching to experimental data. It consisted of variation along $T_{1,b}$ ([1500 : 100 : 1900] ms), $T_{1,t}$ ([600 : 50 : 2000] ms), v_b ([1 : 1 : 10]%), τ_b ([200 : 100 : 1600]ms) and B_1^+ ([0.7 : 0.02 : 1.2]). In addition to this an

additional $T_{1,t}$ value of 3000 ms was included to account for CSF that may still be present post masking for partial volume effects. Matching was performed using the inner-product method.¹³ The step sizes were chosen with consideration to computational and temporal feasibility and parameter ranges to encompass the physiologically relevant ranges.

Matching of B_1^+ and T_1 simultaneously poses a challenge in MRF due to difficulties in separating differences in signal due to T_1 changes from those due to B_1^+ changes when the signal is normalized.^{35–37} Erroneously high matched B_1^+ values are reported around the center of the brain, visible in Figure 3: this effect is prominent at higher B_1 values. These “spikes” in B_1^+ have a knock on effect on the remaining parameters. This was alleviated by performing a multistage matching process and utilizing the knowledge that B_1^+ varies smoothly across the image. Standard matching was performed across the data and the B_1^+ map isolated. The corrupted high B_1^+ values were then removed (B_1^+ values that fell above the 90th percentile of matched values). The remaining B_1^+ map was fitted by triangulating the input data³⁸ and constructing a piecewise cubic interpolating Bezier polynomial on each triangle.³⁹ This new B_1^+ map was further smoothed using a Gaussian filter with a SD of 1.5 pixels and then re-discretized to the coarseness of the dictionary and fixed for each voxel. A second match was performed with fixed B_1^+ values to generate the corresponding remaining parameter maps.

After matching, the median value across each segment identified by the SynthSeg segmentation was taken. Repeatability assessment involved generation of Bland-Altman plots of each parameter and calculation of their repeatability coefficient (RC).⁴⁰

2.2.4 | Noise metric

SNR for experimental results was defined as the mean value of the signal across the time course in each voxel

divided by the residual sum of squares between the experimental signal and its closest dictionary match:

$$\text{SNR} = \frac{\bar{x}}{\sum_{i=0}^{N_{\text{tot}}} (x_i - y_i)^2}, \quad (5)$$

where x and y are the experimental signal and its closest dictionary match, respectively, and N_{tot} is the total number of applied TRs. This provides a measure by which to compare simulated and experimental results.

2.2.5 | Statistical analysis

Statistical analysis of the repeatability was performed using the RC and intra-class correlation coefficient (ICC). RC provides the expected difference in value between two repeats within 95% confidence limits,⁴¹ while ICC describes the resemblance between two groups scaled between 0 and 1.⁴² The scale described by Koo and Li⁴³ was used to characterize ICC scores: less than 0.50 – poor, between 0.50 and 0.75 – moderate, between 0.75 and 0.90 – good, greater than 0.90 – excellent.

3 | RESULTS

3.1 | Simulation experiments

The optimized values governing α and TR were found to be $\alpha_{\text{max}} = 52$ degrees, $w_\alpha = 40\pi$ # of TRs, $f = 181$ (#of TR)⁻¹, $\text{TR}_{\text{min}} = 100$ ms, and $\text{TR}_{\text{max}} = 190$ ms. A visualization of these variations in α and TR can be seen in Figure 2C,D. The sensitivity of this optimized sequence to water exchange can be seen in Figure 4. While the changes in the signal are small, the high level of sampling of the MRF images and the distinct pattern of variation that is characteristic to water exchange changes allow for these parameters to be matched.

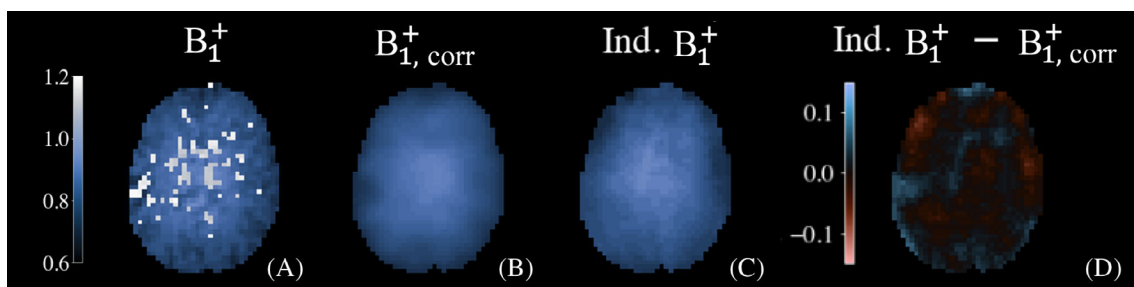
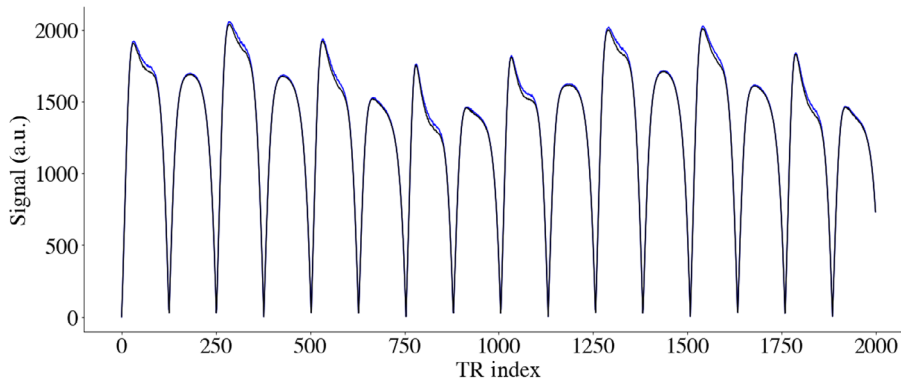


FIGURE 3 (A) B_1^+ map quantified simultaneously with $T_{1,t}$, $T_{1,b}$, τ_b , and v_b using the standard matching technique¹³ and (B) the proposed B_1^+ corrected matching technique. Additionally, (C) an independently acquired B_1^+ map and (D) the subtraction between the independently acquired and corrected map.

FIGURE 4 Two normalized dictionary entries with $\tau_b = 200$ s (blue) and 1600 ms (black), with other parameters fixed. These signals have the fixed parameters, $v_b = 4\%$, $T_{1,t} = 1300$ ms, $T_{1,b} = 1700$ ms, $B_1^+ = 1.0$.



When implementing a 2D dictionary with no variation in $T_{1,t}$, $T_{1,b}$, or B_1^+ values, quantification was most robust to noise in the presence of large blood volumes and long residence times (low exchange), seen in Figure 6A. When variation is present in $T_{1,t}$ and $T_{1,b}$, and B_1 , assuming literature values leads to large errors regardless of noise levels, Figure 6B: neither v_b or τ_b are quantifiable under these conditions in a noise-free simulation, with a mean deviation from the ground truth in matching of 4.4% and 715 ms for v_b and τ_b , respectively.

Using the 5D dictionary (Figure 6C), results in less noise in the matched values than when using the 2D dictionary (Figure 5) across both v_b and τ_b ; this is due to averaging effects in the larger dictionary (the 5D dictionary is 90 times larger than its 2D counterpart). Comparing the matching success of v_b and τ_b between the 2D and 5D dictionaries we can see that there is no significant difference in accuracy ($\sigma_G = [0.06, 0.09]$, $v_b : p = [0.2745, 0.0562]$, $\tau_b : p = [0.1590, 0.2311]$, t-test) or precision ($\sigma_G = [0.06, 0.09]$, $v_b : p = [0.1396, 0.2245]$, $\tau_b : p = [0.2360, 0.6370]$, t-test) between the dictionaries. For this level of dictionary coarseness, no error is seen in the matching of $T_{1,t}$, $T_{1,b}$, or B_1^+ at these noise levels.

Figure 6 illustrates the SNR required to successfully quantify v_b and τ_b when using the 5D dictionary. Looking at the mean deviation of the matched value from the ground truth for both v_b and τ_b across the dictionary, and imposing a threshold of success of a mean deviation of half a dictionary step size or less, we can see that v_b can be quantified accurately up to a noise level equal to $\sigma_G = 0.07$ (corresponding to an SNR of 1.9), while the τ_b is only quantifiable up to a noise level of $\sigma_G = 0.04$ (SNR of 3.3).

3.2 | Healthy volunteer testing

The above simulation results informed the quantification of the healthy volunteer data: voxels with an SNR of less than 3.3 were removed from calculations (mean SNR across volunteers was 11.86). The maps of removed voxels can be seen in Figure S2.

Maps of $T_{1,t}$, $T_{1,b}$, B_1^+ , v_b , and τ_b for a single volunteer alongside their repeat scan can be seen in Figure 7. Maps for all volunteers can be seen in Figure S3. Maps of each parameter are visually consistent between repeats and between individuals. Regional variation is apparent in the maps of $T_{1,t}$ and v_b , while all other maps show little spatial variation. The patterns of spatial variation are largely consistent between scans for $T_{1,t}$, while the spatial distribution of v_b is visually less repeatable.

The mean values for each parameter across the ten subjects can be seen in Figure 8. Mean $T_{1,t}$ differed between white and gray matter (1060 ± 50 and 1290 ± 70 ms, respectively [$p < 0.0001$], paired t-test), as did mean v_b ($1.9 \pm 0.4\%$ and $2.8 \pm 0.7\%$, respectively [$p < 0.0001$], paired t-test). $T_{1,b}$ values were highly similar for white and gray matter (1750 ± 10 ms and 1756 ± 10 ms, respectively [$p = 0.4270$], paired t-test), as were τ_b (930 ± 100 and 950 ± 150 ms, respectively [$p = 0.6609$], paired t-test).

Bland–Altman plots (Figure 9) show the scan–rescan variation in mean parameter values for white matter and gray matter. Negligible bias is observed between measurements. RC and intraclass correlation coefficients for each parameter are shown in Table 1. The ICC indicates good to excellent levels of repeatability for all parameters except $T_{1,b}$ where the repeatability is moderate for gray matter and white matter.

4 | DISCUSSION

4.1 | Simulation experiments

The simulation-based optimization of the data acquisition focused on optimizing the patterns of flip angle and repetition time variation. A parametric form was used to enable optimization that included five parameters controlling the height and width of regularly shaped curves (Equations 2, 3 and Figure 2A,B). This approach has the advantage of simplicity and ease of optimization, but it limits the potential patterns of variation to those that can

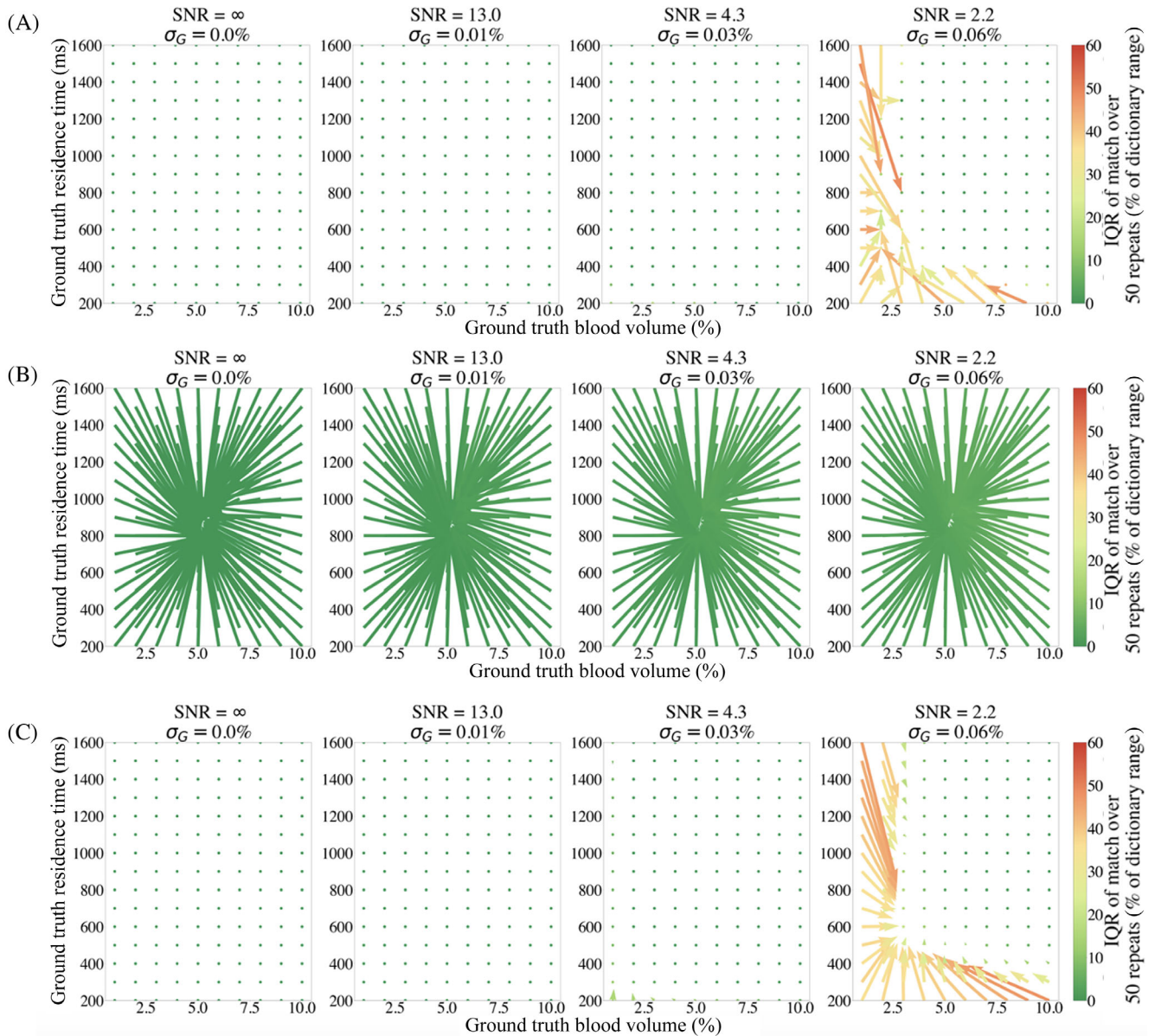


FIGURE 5 The success of matching a fingerprint to its corresponding dictionary entry for (A) v_b and τ_b with a fixed $T_{1,b}$, $T_{1,t}$, B_1^+ , (B) v_b and τ_b when there is discrepancy in the assumed values for $T_{1,b}$, $T_{1,t}$, B_1^+ , and (C) v_b , τ_b , $T_{1,b}$, $T_{1,t}$, and B_1^+ simultaneously. Each plot displays the two-dimensional dictionary laid out with each residence time (τ_b) and blood volume (v_b) combination. Arrows indicate the deviation in matching from the ground truth value—the bottom of arrow is situated at the true value, the tip at median matched value. The interquartile range (IQR) of matching across 50 repetitions is indicated by the color of the arrow. Absence of arrows indicates perfect matching. This can be seen across four example noise levels, σ_G , corresponding to the SD of the Gaussian noise added to the signal. (A) Experiment 1. Data: 2D (v_b , τ_b). Dictionary 2D (v_b , τ_b); (B) Experiment 2. Data: 5D ($T_{1,b}$, $T_{1,t}$, B_1^+ , v_b , τ_b). Dictionary 5D (v_b , τ_b); (C) Experiment 3. Data: 5D ($T_{1,b}$, $T_{1,t}$, B_1^+ , v_b , τ_b). Dictionary 5D ($T_{1,b}$, $T_{1,t}$, B_1^+ , v_b , τ_b).

be parameterized using these simple functions. Due to the optimization of the parameter variation relying on the difference between two separately generated signals, common techniques that contain a random element, such as Perlin noise variations,⁴⁴ were avoided. Other work has focused on a free-form optimization of input parameters using the Cramer–Rao bound objective function.^{45,46} However, due to the high dimensionality of our optimization

problem, the computational and time requirements render this unfeasible.

Lack of success of quantification is seen when there is variation in $T_{1,t}$, $T_{1,b}$, and B_1^+ that is not accounted for. Inaccurately matched values of dictionary-based matching techniques inherently tend toward the average signal, in the case of a uniformly sampled dictionary, the central value. This suggests that, unless independent measures of

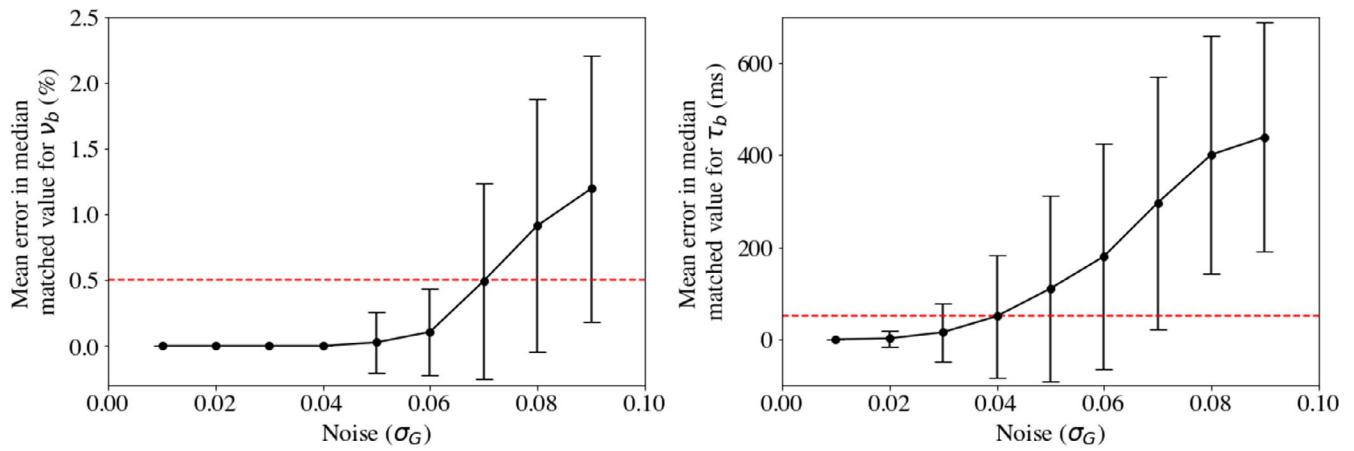


FIGURE 6 The success of quantifying (A) v_b and (B) τ_b across different noise levels. The matching is considered to have failed when the mean difference in the median matched value from the ground truth is larger than half a dictionary step size: this threshold is marked by the dotted red line.

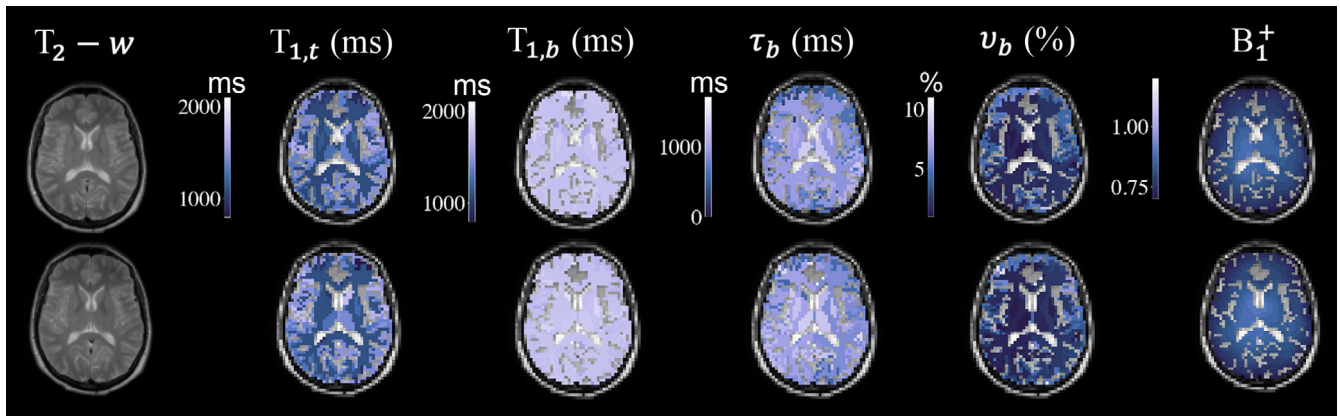


FIGURE 7 Regional quantitative parameter maps of $T_{1,t}$, $T_{1,b}$, v_b and τ_b for a single volunteer with repeat scan, and a voxel-wise map for B_1^+ .

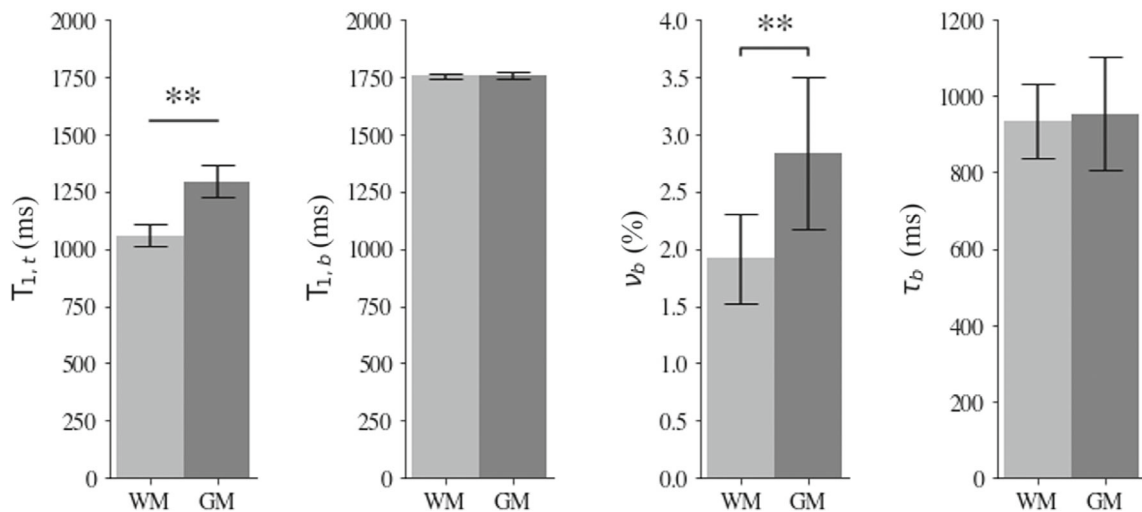


FIGURE 8 Global white and gray matter values averaged across all 10 volunteers. Asterisks represent differences with $p < 0.0001$, paired t-test.

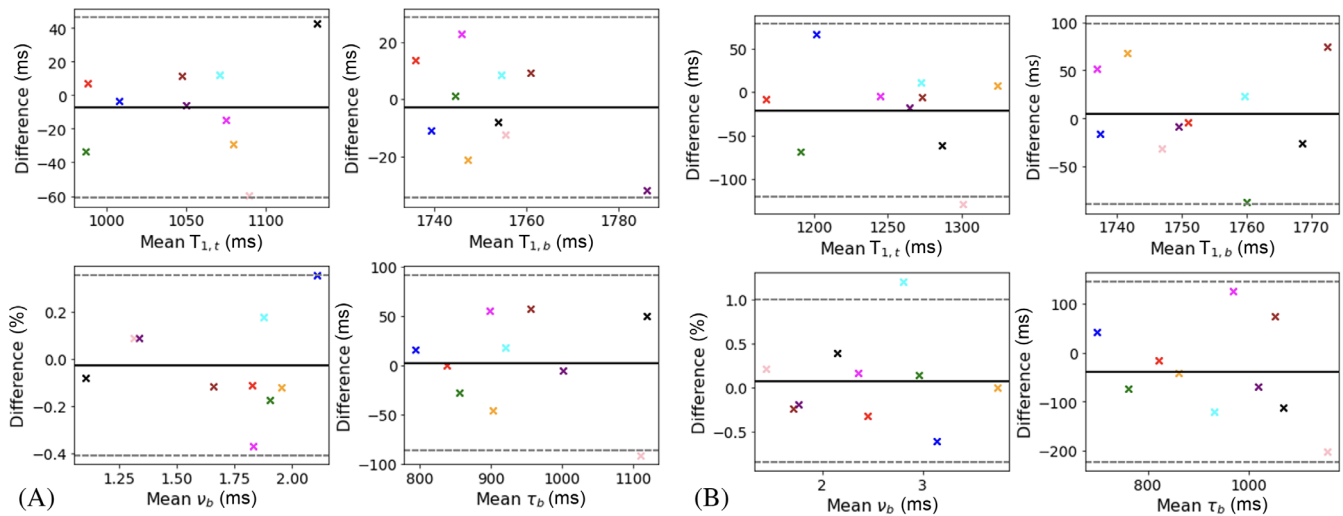


FIGURE 9 Bland–Altman plot comparing repeat measurements for $T_{1,t}$, $T_{1,b}$, B_1^+ , v_b , and τ_b for (A) white matter, and (B) cortical gray matter. Marker color is consistent across plots for each volunteer. Solid black line indicates mean difference between scan/rescan, with the 95% limits of agreement shown with dashed lines.

TABLE 1 The mean values, repeatability coefficient and intraclass correlation coefficient for white and gray matter across the four quantified tissue parameters.

	WM			GM		
	Mean	RC	ICC	Mean	RC	ICC
$T_{1,t}$ (ms)	1060	38.70	0.92	1290	67.59	0.89
$T_{1,b}$ (ms)	1750	22.01	0.56	1750	23.61	0.59
v_b (%)	1.9	0.44	0.85	2.8	0.48	0.94
τ_b (ms)	930	45.74	0.97	950	108.75	0.94

Abbreviations: GM, gray matter; ICC, intraclass correlation coefficient; RC, repeatability coefficient; WM, white matter.

these parameters are provided, all five parameters need to be quantified simultaneously using a 5D dictionary.

In order to reduce the dimensionality of the problem posed here an RF spoiled gradient echo sequence was selected with a short TE = 2.1 ms. This removes dependence of the signal on T_2^* , reducing the number of parameters that need to be quantified simultaneously.

The largest limitation of the underlying model (as with any model) is that the pathology of the human brain is far too complex to simulate in its entirety. This means that models can only account for a select few effects on signals, with the intention that these effects describe the meaningful majority of the observed signal variance; a simulation will never be completely accurate. Here, a two compartment generative model is assumed, which neglects, for example, exchange between plasma and red blood cells, and exchange between interstitial fluid and the various cells found in the brain. In addition it is assumed that water is well mixed in each compartment, with exchange being equally probable for spins throughout each compartment,

rather than being more likely for those closer to the BBB. We also assume that blood flow has no influence on the probability of exchange occurring; not including flow in the dictionary was found to not impact the quantification. In all cases it is possible to extend the generative model to account for these additional possibilities, although incorporation into the MRF framework would pose substantial computational challenges.

4.2 | Healthy volunteer testing

This is the first demonstration of MRF methods to provide regional mapping in the human brain of BBB water exchange. All parameters showed good agreement with literature ranges.^{8,18,19,21,22} Expected differences between white and gray matter $T_{1,t}$ and v_b are observed, while no differences are seen in τ_b or $T_{1,b}$. Blood T_1 would be expected to be approximately the same in both tissues, although differences in mean oxygenation may lead

to small differences. It is unclear from the existing literature if we would expect to see differences τ_b regionally, although systematic differences in capillary geometry between white and gray matter could be hypothesized to lead to decreased τ_b in GM due to the increased surface area of vessels.⁴⁷ In lieu of a direct comparison between these results and other known physiological biomarkers, hemispheric agreement was looked at as a metric of the physiological relevance of the information extracted as noise did not appear to be symmetrical across the brain, shown in Figure S3). Across maps good agreement is seen between hemispheres indicating the matching reflects the underlying tissue properties rather than noise-based fluctuations. Variation in τ_b and v_b can be seen in the frontal lobes compared to the other regions in the brain across volunteers. This is likely not a physiological phenomenon but due to distortions in the area resulting from a susceptibility artifact from the eyes. Little bias and generally good precision is observed within and across regions. The quantification of gray matter parameters was less robust than the white matter parameters, which is likely due to the slice chosen including a relatively small volume of gray matter, leading to fewer voxels to average over. Gray matter is more likely to suffer from partial volume from white matter and CSF, which may explain the slightly low blood volume estimates and lower repeatability.

The data presented here are regionally averaged, as the voxel-wise data are noisy. However, it is possible that denoising strategies may mitigate this impact. There are currently few contrast-agent free BBB techniques sensitive enough for the measurement of voxel-wise BBB parameters.⁴⁸ Most report regionally averaged WEX parameters.^{12,49} Even when voxel-wise values are reported these are noisy. Despite this, the test-retest repeatability is in line with the values reported by a recent BBB-arterial spin labeling study.⁴⁸

In addition, when the error in the matching is evaluated (Figure S4), it can be seen that noise in the images contains a strong coherent component that predominantly affects the anterior right of the brain surrounding the ventricles. This may be attributed to a previously identified issue with ordering of the spiral interleaves during reconstruction⁵⁰ and CSF pulsation. The coherent nature of this artifact causes bias in the data, disrupting matching. Implementation of a modified reconstruction or denoising technique could be applied to alleviate this issue.

A limitation of implementing this work in clinical populations is the length of the acquisition, at 19 min, and in this work only a single slice is acquired due to limitations in the base MRF sequence that the protocol was constructed with. However, due to the short TE and long TRs used, multislice acquisition could be implemented in

this time.^{51,52} While the length of the MRF acquisition is long is it comparable to some published BBB acquisitions.¹² While these times are for whole brain acquisitions, this sequence could be modified to cover most of the brain in the same time.

MRF is known to be particularly robust to incoherent noise and motion due to the inner-product matching method employed¹³: this gives a benefit over other techniques when it comes to accurate quantification over long scan times. Acceleration strategies, such as in-place parallel reconstruction and simultaneous multislice methods may also prove to be beneficial: simultaneous multislice would allow for multiple slices to be acquired in the same acquisition time. While the length of the MRF acquisition is long, published BBB acquisition techniques range from half this acquisition time¹² to approximately the same length.⁴⁸ Measurement of a water exchange using the current sequence requires relatively long TRs to allow for enough exchange to occur for measurement. If increasing the numbers TRs would be required, further sequence development and optimization would be recommended to gain sensitivity at shorter TRs to reduce scan time.

A key limitation of using MRF for the quantification of any parameter is the inherently discrete nature of the quantification. The dictionary to which the experimental data is matched is finite, and due to computational constraints often modest, which leads to discretization errors in the final maps. This problem is a topic of much interest in the field, particularly in high dimensional problems such as this one. Application of machine learning algorithms has been used to alleviate this issue⁵³⁻⁵⁵ and may be of benefit to our proposed approach.

5 | CONCLUSIONS

Our simulations suggest that it is possible to optimize an RF spoiled gradient echo-MRF acquisition for the quantification of blood volume and residence time of water in blood, simultaneously with $T_{1,b}$, $T_{1,t}$, and B_1^+ . Our initial findings in healthy volunteers suggest that it is feasible to regionally quantify cerebral blood volume (v_b) and mean intravascular residence time (τ_b), simultaneously with $T_{1,b}$, $T_{1,t}$, and B_1^+ using an RF spoiled gradient echo-MRF acquisition within a reasonable scan time. Our approach holds promise for patient-based measurements of subtle BBB disruption.

ACKNOWLEDGMENTS

The authors wish to thank Dr. David Higgins and Julia Markus for their help implementing this work in vivo.

CONFLICT OF INTEREST STATEMENT

Geoff J. M. Parker declares the following potential conflicts of interests in companies with an interest in imaging biomarkers: Director and shareholder in Bioxydyn Limited; Director and shareholder in Quantitative Imaging Limited; Director and shareholder in Queen Square Analytics Limited. Claudia A. M. Gandini Wheeler-Kingshott is a shareholder in Queen Square Analytics Limited.


DATA AVAILABILITY STATEMENT

Sample data and the code used to generate the results presented in this paper are available at https://github.com/EmmaThomson/MRFSGRE_BBB.

ORCID

Emma L. Thomson  <https://orcid.org/0000-0003-1840-8509>

Elizabeth Powell  <https://orcid.org/0000-0002-1059-1188>

Claudia A. M. Gandini Wheeler-Kingshott  <https://orcid.org/0000-0002-4832-1300>

Geoff J. M. Parker  <https://orcid.org/0000-0003-2934-2234>

REFERENCES

- Daneman R, Prat A. The blood-brain barrier. *Cold Spring Harb Perspect Biol.* 2015;7:a020412.
- Zlokovic BV. The blood-brain barrier in health and chronic neurodegenerative disorders. *Neuron.* 2008;57:178-201.
- Tofts PS, Kermode AG. Measurement of the blood-brain barrier permeability and leakage space using dynamic MR imaging. 1. Fundamental concepts. *Magn Reson Med.* 1991;17:357-367.
- Heye AK, Thrippleton MJ, Armitage PA, et al. Tracer kinetic modelling for DCE-MRI quantification of subtle blood-brain barrier permeability. *Neuroimage.* 2016;125:446-455.
- Kanda T, Ishii K, Kawaguchi H, Kitajima K, Takenaka D. High signal intensity in the dentate nucleus and globus pallidus on unenhanced T1-weighted MR images: relationship with increasing cumulative dose of a gadolinium-based contrast material. *Radiology.* 2014;270:834-841.
- Keisuke Y, Liu CH, Faraco G, et al. Size-selective opening of the blood-brain barrier by targeting endothelial sphingosine 1-phosphate receptor 1. *Proc Natl Acad Sci USA.* 2017;114:4531-4536.
- Nitta T, Hata M, Gotoh S, et al. Size-selective loosening of the blood-brain barrier in claudin-5-deficient mice. *J Cell Biol.* 2003;161:653-660.
- Dickie BR, Parker GJM, Parkes LM. Measuring water exchange across the blood-brain barrier using MRI. *Prog Nucl Magn Reson Spectrosc.* 2020;116:19-39.
- Li Y, Li M, Zuo L, et al. Compromised blood-brain barrier integrity is associated with total magnetic resonance imaging burden of cerebral small vessel disease. *Front Neurol.* 2019;9:221. <https://www.ncbi.nlm.nih.gov/pmc/articles/PMC5897516/pdf/fneur-09-00221.pdf>
- St Lawrence KS, Owen D, Wang DJJ. A two-stage approach for measuring vascular water exchange and arterial transit time by diffusion-weighted perfusion MRI. *Magn Reson Med.* 2012;67:1275-1284.
- Bai R, Li Z, Sun C, Hsu YC, Liang H, Basser P. Feasibility of filter-exchange imaging (FEXI) in measuring different exchange processes in human brain. *Neuroimage.* 2020;219:117039.
- Powell E, Ohene Y, Battiston M, Dickie BR, Parkes LM, Parker GJM. Blood-brain barrier water exchange measurements using FEXI: impact of modeling paradigm and relaxation time effects. *Magn Reson Med.* 2023;90:34-50.
- Ma D, Gulani V, Seiberlich N, et al. Magnetic resonance fingerprinting. *Nature.* 2013;495:187-192.
- Panda A, Mehta BB, Coppo S, et al. Magnetic resonance fingerprinting - an overview. *Curr Opin Biomed Eng.* 2017;3:55-66.
- Jakob A. A perspective on MR fingerprinting. *J Magn Reson Imaging.* 2020;53:676-685.
- Abo SS. *Code to Design Multiband RF Pulses.* GitHub; 2019. <https://github.com/mriphysics/Multiband-RF>
- Little JDC, Murty KG, Sweeney DW, Karel C. An algorithm for the traveling salesman problem. *Oper Res.* 1963;11:972-989.
- Wansapura JP, Holland SK, Dunn RS, Ball WS. NMR relaxation times in the human brain at 3.0 tesla. *J Magn Reson Imaging.* 1999;9:531-538.
- Lin C, Bernstein M, Hudson J, Fain S. Measurement of T1 relaxation times at 3.0T: implications for clinical MRA. Paper presented at: Proceedings of the 9th International Society of Magnetic Resonance in Medicine. 2001:1391.
- Zhang X, Petersen ET, Ghariq E, et al. In vivo blood T1 measurements at 1.5T, 3T, and 7T. *Magn Reson Med.* 2013;70:1082-1086.
- Grubb RL, Raichle ME, Higgins CS, Eichling JO. Measurement of regional cerebral blood volume by emission tomography. *Ann Neurol.* 1978;4:322-328.
- Lee C, Baker E, Thomsson D. Normal regional T1 and T2 relaxation times of the brain at 3T. Paper presented at: Proceedings of the 14th International Society of Magnetic Resonance in Medicine. 2006:959.
- Stanisz GJ, Odobina EE, Pun J, et al. T1, T2 relaxation and magnetisation transfer in tissue at 3T. *Magn Reson Med.* 2005;54:507-512.
- Ethofer T, Mader I, Seeger U, et al. Comparison of longitudinal metabolite relaxation times in different regions of the human brain at 1.5T and 3T. *Magn Reson Med.* 2003;50:1296-1301.
- Greenman RL, Shirosky JE, Mulkern RV, Rofsky NM. Double inversion black-blood fast spin-Echo imaging of the human heart: a comparison between 1.5T and 3.0T. *J Magn Reson Imaging.* 2003;17:648-655.
- Lu H, Clingman C, Golay X, Van Zijl PCM. Determining the longitudinal relaxation time (T1) of blood at 3.0 tesla. *Magn Reson Med.* 2004;52:679-682.
- Petrovic A, Krauskopf A, Hassler E, Stollberger R, Scheurer E. Time related changes of T1, T2, and T2* of human blood in vitro. *Forensic Sci Int.* 2016;262:11-17.
- Bojorquez JZ, Bricq S, Acquitter C, Brunotte F, Walker PM, Lalande A. What are normal relaxation times of tissue at 3T? *Magn Reson Imaging.* 2017;35:69-80.
- Smith SM. Fast robust automated brain extraction. *Hum Brain Mapp.* 2002;17:143-155.
- Jenkinson M, Smith SM. A global optimisation method for robust affine registration of brain images. *Med Image Anal.* 2001;5:143-156.

31. Mark J, Peter B, Michael B, Smith SM. Improved optimisation for the robust and accurate linear registration and motion correction of brain images. *Neuroimage*. 2002;17:825-841.
32. Woolrich MW, Jbabdi S, Patenaude B, et al. Bayesian analysis of neuroimaging data in FSL. *Neuroimage*. 2009;45:S173-S186.
33. Andersson JLR, Jenkinson M, Smith SM. Non-linear registration, aka spatial normalisation. FMRIB Technical Report No. TR07JA2. 2010.
34. Billot B, Colin M, Arnold SE, Das S, Iglesias JE. Robust segmentation of brain MRI in the wild with hierarchical CNNs and no Retraining. *arxiv.2203.01969*. 2022.
35. Buonincontri G, Sawiak SJ. MR fingerprinting with simultaneous B1 estimation. *Magn Reson Med*. 2016;76:1127-1135.
36. Chen Y, Jiang Y, Pahwa S, et al. MR fingerprinting for rapid quantitative abdominal imaging. *Radiology*. 2016;279:278-286.
37. Ma D, Coppo S, Chen Y, et al. Slice profile and B1 corrections in 2D magnetic resonance fingerprinting. *Magn Reson Med*. 2017;78:1781-1789.
38. Barber CB, Dobkin DP, Huhdanpaa HT. The Quickhull algorithm for convex hulls. *ACM Trans Math Softw*. 1996;22:469-483.
39. Peter A. A trivariate Clough-Tocher scheme for tetrahedral data. *ACM Trans Math Softw*. 1984;1:169-181.
40. Vaz S, Falkmer T, Passmore AE, Parsons R, Andreou P. The case for using the repeatability coefficient when calculating test-retest reliability. *PLoS One*. 2013;8:e73990.
41. Institution British Standards. *British Standard: Precision of Test Methods: Part 1. Guide for the Determination of Repeatability and Reproducibility for a Standard Test Method by Inter-Laboratory Tests*. B.S. (Series) British Standards Institution; 1987.
42. Gary K. *Intraclass Correlation Coefficient*. Springer; 2006.
43. Koo TK, Li MY. A guideline of selecting and reporting intraclass correlation coefficients for reliability research. *J Chiropr Med*. 2016;15:155-163.
44. Ken P. An image synthesizer. *Comput Graph*. 1985;19:287-296.
45. Zhao B, Setsompop K, Ye H, Cauley SF, Wald LL. Maximum likelihood reconstruction for magnetic resonance fingerprinting. *IEEE Trans Med Imaging*. 2016;35:1812-1823.
46. Bo Z, Kawin S, Elfar A, et al. Improved magnetic resonance fingerprinting reconstruction with low-rank and subspace modeling. *Magn Reson Med*. 2018;79:933-942.
47. Kubíková T, Kochová P, Tomášek P, Witter K, Tonar Z. Numerical and length densities of microvessels in the human brain: correlation with preferential orientation of microvessels in the cerebral cortex, subcortical grey matter and white matter, pons and cerebellum. *J Chem Neuroanat*. 2018;88:22-32.
48. Mahroo A, Buck MA, Huber J, et al. Robust multi-TE ASL-based blood-brain barrier integrity measurements. *Front Neurosci*. 2021;15:719676.
49. Shao X, Jann K, Ma SJ, et al. Comparison between blood-brain barrier water exchange rate and permeability to gadolinium-based contrast agent in an elderly cohort. *Front Neurosci*. 2020;14:571480.
50. Kördörfer G, Pfeuffer J, Kluge T, et al. Effect of spiral under-sampling patterns on FISP MRF parameter maps. *Magn Reson Imaging*. 2019;62:174-180.
51. Haar HJ, Saartje B, Hofman Paul AM, Verhey Frans RJ, Jansen Jacobus FA, Backes WH. Multiple-line-scanning spin density imaging. *J Magn Reson*. 1980;41:112-126.
52. Barth M, Breuer F, Koopmans PJ, Norris DG, Poser BA. Simultaneous multislice (SMS) imaging techniques. *Magn Reson Med*. 2016;75:63-81.
53. Song P, Eldar YC, Mazor G, Rodrigues MRD. HYDRA: hybrid deep magnetic resonance fingerprinting. *Med Phys*. 2019;46:4951-4969.
54. Cohen O, Zhu B, Rosen MS. MR fingerprinting deep RecOnstruction NEtwork (DRONE). *Magn Reson Med*. 2018;80:885-894.
55. Hoppe E, Korzdorfer G, Wurfl T, et al. Deep learning for magnetic resonance fingerprinting: a new approach for predicting quantitative parameter values from time series. *Stud Health Technol Inform*. 2017;243:202-206.

SUPPORTING INFORMATION

Additional supporting information may be found in the online version of the article at the publisher's website.

Figure S1. Replication of Figure 6, error in matching success when noisy simulated signals are matched to a dictionary, now with flow included in the simulation. Flow was introduced by including incoming spins that enter the blood compartment with a magnetization equal to the initial magnetization. The rate of inflow was dictated by a mean transit time. (MTT = 2800 ms) At the same rate, out-flowing spins were continually tracked, and experienced relaxation without exchanging. No significant difference is seen in these matching successes and those without flow consideration (Figure 6): $p = 0.154$ and 1 for v_b and $p = 0.909$ and 0.051 for τ_b for $\sigma_G = 0.06$, and 0.09 respectively, suggesting that the inclusion of flow does not significantly affect estimation error.

Figure S2. Red voxels represent areas of low SNR that will result in a fit failure for τ_b and are therefore removed from calculations for all volunteers.

Figure S3. Regional quantitative parameter maps of $T_{1,t}$, $T_{1,b}$, v_b and τ_b for all volunteers with repeat scan, and a voxel wise map for B_1^+ .

Figure S4. Voxel wise maps of match quality for all volunteers represented by the residual sum of squares between the experimental signal and its closest dictionary match. Areas with a larger RSS are noisier.

How to cite this article: Thomson EL, Powell E, Gandini Wheeler-Kingshott CAM, Parker GJM. Quantification of water exchange across the blood-brain barrier using noncontrast MR fingerprinting. *Magn Reson Med*. 2024;92:1392-1403. doi: 10.1002/mrm.30127